

# ViP3D: End-to-end Visual Trajectory Prediction via 3D Agent Queries

Junru Gu<sup>1\*</sup>   Chenxu Hu<sup>1\*</sup>   Tianyuan Zhang<sup>2,3</sup>   Xuanyao Chen<sup>2,4</sup>

Yilun Wang<sup>5</sup>   Yue Wang<sup>6</sup>   Hang Zhao<sup>1,2†</sup>

<sup>1</sup>IIIS, Tsinghua University   <sup>2</sup>Shanghai Qi Zhi Institute

<sup>3</sup>CMU   <sup>4</sup>Fudan University   <sup>5</sup>Li Auto   <sup>6</sup>MIT

**Abstract:** In the existing autonomous driving systems, perception and prediction are two separate modules. The two modules communicate via hand-picked features such as agent boxes and trajectories as interfaces. Due to this separation, the prediction module only receives limited information from the perception module. Even worse, errors from the perception modules can propagate and accumulate, adversely affecting the prediction results. In this work, we propose ViP3D, a query-based visual trajectory prediction pipeline that exploits rich information from raw videos to predict future trajectories of agents in a scene. ViP3D employs sparse agent queries throughout the pipeline, making it fully differentiable and interpretable. Extensive experimental results on the nuScenes dataset show the strong performance of ViP3D over traditional pipelines and previous end-to-end models.<sup>1</sup>

**Keywords:** Trajectory Prediction, Autonomous Driving, End-to-End Learning

## 1 Introduction

An autonomous driving system should be able to perceive agents in the current environment and predict their future behaviors, so that the autonomous vehicle could navigate the world safely. Perception and prediction are two separate modules in the existing software pipelines, where the interface between them is often defined by hand-picked features, such as historical agent trajectories, agent types, agent sizes, *etc.* Such construction leads to a loss of perceptual information that is useful for trajectory prediction. For example, tail lights and brake lights indicate a vehicle’s intention, a pedestrian’s head pose and body pose tell about his/her attention. Such information, if not explicitly modeled, is ignored in the existing pipeline. In addition, with the separation of perception and prediction, errors are accumulated and cannot be cured in later stages. Specifically, historical trajectories used by trajectory predictors come from an upstream perception module, which inevitably contains errors, leading to a drop in the prediction performance. Designing a trajectory predictor that is robust to upstream output errors is a non-trivial task [1].

Recent works such as IntentNet [2], FaF [3], PnPNet [4] propose end-to-end models for LiDAR-based trajectory prediction. However, they are not able to leverage the abundant visual information from cameras. What is worse, these models rely on convolutional neural networks which use feature maps as their intermediate representations, thus suffering from non-differentiable post-processing operations, e.g., non-maximum suppression in detection and object association in tracking.

To address all these challenges, we propose a novel pipeline, dubbed **ViP3D** (Visual trajectory Prediction via **3D** agent queries). ViP3D consumes image sequence from surrounding cameras and high-definition map, and makes instance-wise future trajectory prediction in an end-to-end

---

\*Equal contribution.

†Corresponding to: hangzhao@mail.tsinghua.edu.cn

<sup>1</sup>Project page: <https://tsinghua-mars-lab.github.io/ViP3D>

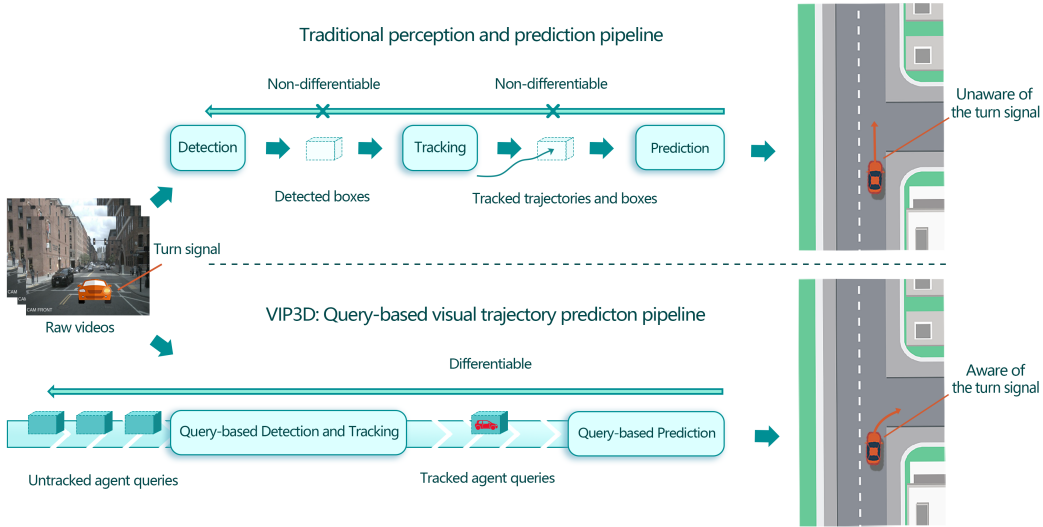


Figure 1: Comparison of a traditional multi-stage cascaded pipeline and ViP3D. The traditional pipeline involves multiple non-differentiable modules, e.g., detection, tracking, and prediction. ViP3D takes multi-view videos as input and generates predicted trajectories in an end-to-end manner, which can effectively leverage visual information such as turning signals of vehicles.

and streaming manner. Specifically, ViP3D leverages 3D agent queries as interface throughout the pipeline, where each query can map to (at most) an agent in the environment. At each time step, the queries aggregate visual features from multi-view images, learn agent temporal dynamics, model the relationship between agents, and finally produce possible future trajectories for each agent. Across time, the 3D agent queries are maintained in a memory bank, which can be updated, discarded and renewed, making it an efficient streaming approach.

In summary, the contribution of this paper is three-fold:

1. ViP3D is the first **fully differentiable vision-based** approach to predict future trajectories of agents for autonomous driving. Compared with hand-picked features like historical trajectories and agent sizes, visual features can implicitly encode rich and fine-grained information which is useful for the trajectory prediction task.
2. With 3D agent queries as interface, ViP3D explicitly models **instance-wise** agent detection, tracking and prediction, making it **interpretable** and **debuggable**.
3. ViP3D is an efficient **streaming** model with **high performance**. It outperforms a wide variety of baselines and recent end-to-end methods on the visual trajectory prediction task.

## 2 Related Work

**3D Detection.** There are a great number of works on 3D object detection and tracking from point clouds [5, 6, 7]. In this paper, we focus on 3D detection and tracking from cameras. Monodis [8] and FCOS3D [9] learns a single-stage object detector with instance depth and 3D pose predictions on monocular images. Pseudo-LiDAR [10] first predicts depth for each image pixel, then lifts them into the 3D space, and finally employs a point cloud based pipeline to perform 3D detection. DETR3D [11] designs a sparse 3D query-based detection model that maps queries onto 2D multi-view images to extract features. BEVFormer [12] further proposes a dense query-based detection model.

**3D Tracking.** The majority of 3D tracking approaches follow the tracking-by-detection pipeline [13, 14]. These methods first detect 3D objects, then associate existing tracklets with the new detections. CenterTrack [15, 16] uses two consecutive frames to predict the speed of each detection box, then performs association using only  $\ell_2$  distances of the boxes. Samuel *et al.* [17] uses PMBM filter to estimate states of tracklets and match them with new observations. DEFT [18] uses a learned appearance matching network for association, together with an LSTM estimated motion to eliminate implausible trajectories. QD3DT [19] uses cues from depth-ordering and learns better appearance features via contrastive learning. MUTR3D [20] introduces track queries to model objects that appear in multiple cameras across multiple frames.

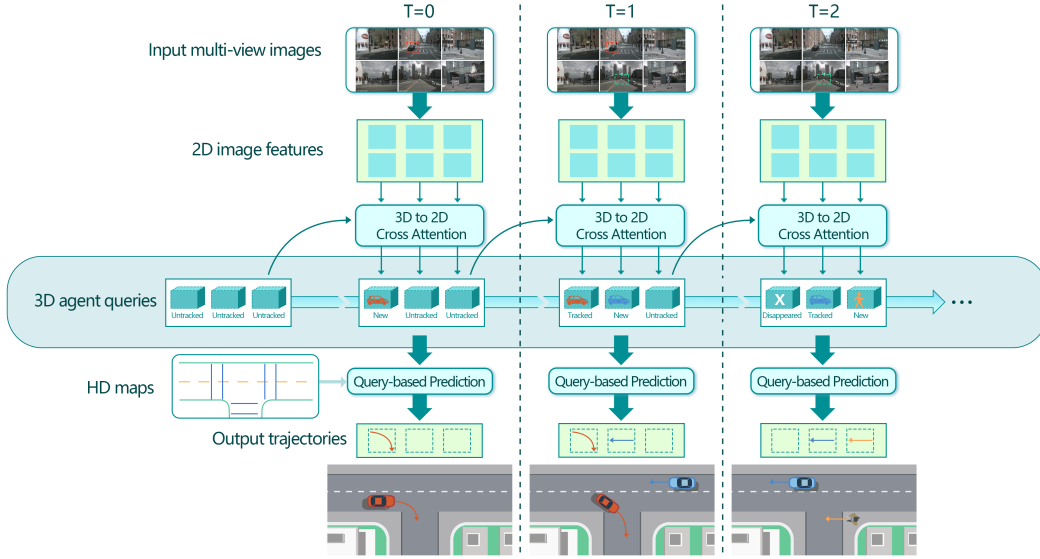


Figure 2: ViP3D architecture. At each time step, 3D agent queries aggregates visual features from multi-view images to obtain tracked agent queries. The queries further interact with HD maps, and are decoded into predicted trajectories. Over time, 3D agent queries are managed in a dynamic memory bank and the model works in a streaming manner.

**Trajectory Prediction.** Most trajectory prediction works focus on modeling the uncertainty of unknown intents and behaviors of agents. Variety loss is a regression-based method that only optimizes the closest predicted trajectory during training. Modeling uncertainty using latent variables [21, 22, 23, 24] is another popular approach, which predicts different future trajectories by randomly sampling from the latent variables. Goal-based methods recently achieve outstanding performance by first predicting intentions of agents, such as the endpoint of trajectories [25, 26, 27, 28], lanes to follow [29, 30, 31], and then predicting future trajectories conditioning on these goals.

**End-to-End Perception and Prediction.** In the last couple of years, there has been growing interest in jointly optimizing detection, tracking, and prediction. FaF [3] employs a single convolutional neural network to detect objects from LiDAR point clouds, and forecast their corresponding future trajectories. IntentNet [2] adds high-level intention output to this framework. More recently, Phillips *et al.* [32] further learns localization together with perception and prediction. FIERY [33] predicts future BEV occupancy heatmaps from visual data directly. Mostly related to our work is PnPNet [4], which explicitly models tracking in the loop. Our method is related to these methods in the sense that we also perform end-to-end prediction based on sensor inputs. However, they all rely on BEV feature maps or heatmaps as their intermediate representation, which leads to unavoidable non-differentiable operation while going from dense feature maps to instance-level features, such as non-maximum suppression (NMS) in detection, and association in tracking. Our method, on the other hand, employs sparse agent queries as representation throughout the model, greatly improving the differentiability and interpretability.

### 3 Method

ViP3D aims to address the trajectory prediction problem from raw videos in an end-to-end fashion by leveraging 3D agent queries. Given multi-view videos and HD maps, ViP3D predicts future trajectories of all agents in the scene. The overall pipeline of ViP3D is shown in Figure 2. At each time step, a Query-based Detection and Tracking module processes multi-view videos from surrounding cameras to obtain tracked agent queries containing visual features. The visual features in the agent queries capture the motion dynamics and visual characteristics of the agents and the relationships between agents. After that, a Query-based Prediction module takes the tracked agent queries as input and associates them with HD map features, and finally outputs predicted trajectories. Across time, the 3D agent queries are updated, discarded and renewed, making ViP3D to work in an efficient streaming manner.

### 3.1 Query-based Detection and Tracking

As shown in Figure 2, the query-based detection and tracking module extracts visual features from raw videos of surrounding cameras. Specifically, for each frame, we follow DETR3D [11] to extract image features. For temporal feature aggregation, inspired by MOTR [34], we design a query-based tracking scheme with two key steps: query feature update and query supervision. Agent queries are updated across time to model the motion dynamics of agents.

#### 3.1.1 Query Feature Update

Each agent query corresponds to at most one agent that appeared in the scene. We use  $\mathbf{Q}$  to denote a set of agent queries, which are initialized as learnable embeddings with 3D reference points. At each time step, we first extract 2D image features of surrounding cameras via ResNet50 [35] and FPN [36]. Then we project the 3D reference points of agent queries onto the 2D coordinates of multi-view images using camera intrinsic and extrinsic transformation matrices. Finally, we sample the corresponding image features to update the agent queries via cross attention:  $\mathbf{Q}_t = \mathbf{Q}\mathbf{W}^Q, \mathbf{K} = \mathbf{L}\mathbf{W}^K, \mathbf{V} = \mathbf{L}\mathbf{W}^V, \mathbf{A}(\mathbf{Q}_t, \mathbf{K}, \mathbf{V}) = \text{softmax}\left(\frac{\mathbf{Q}_t\mathbf{K}^\top}{\sqrt{d_k}}\right)\mathbf{V}, \mathbf{Q} = \text{FFN}_{\text{upd}}(\mathbf{Q}, \mathbf{A}(\mathbf{Q}_t, \mathbf{K}, \mathbf{V}))$ , where  $\mathbf{W}^Q, \mathbf{W}^K, \mathbf{W}^V \in \mathbb{R}^{d_h \times d_k}$  are the matrices for linear projection,  $t \in \{1, \dots, T\}$  is the current time step,  $d_k$  is the dimension of query / key / value vectors, and  $\mathbf{L}$  is the sampled 2D image features.  $\text{FFN}_{\text{upd}}$  is a two-layer MLP that updates the feature of the queries.

#### 3.1.2 Query Supervision

Since each agent query corresponds to at most one agent, supervision is required at each time step to make sure each query extracts features of the same agent across different historical frames. There are two types of queries. One are the matched queries that have been associated with agents before this time step. The other are the empty queries that have not been associated with any agents. Suppose we have done association at time step  $t - 1$ , and now we perform association at time step  $t$ . For the matched queries, we assign the same agents to them as before:  $\mathbf{Q}_{\text{matched}} \cong \mathcal{A}_{\text{old}}$ , where  $\mathcal{A}_{\text{old}}$  denotes the agents appeared at time step  $t - 1$ . If an agent disappeared at time step  $t$ , we assign an empty label to the query which is associated with that agent at time step  $t - 1$ . For the unmatched queries, we perform a bipartite matching between the unmatched queries and the new agents  $\mathcal{A}_{\text{new}}$  appeared at time step  $t$ :  $\mathbf{Q}_{\text{empty}} \cong \mathcal{A}_{\text{new}}$ .

To perform the bipartite matching, we utilize a query decoder that outputs the center coordinates of each query at time step  $t$ . The pair-wise matching cost [37] between ground truth  $y_i$  and a prediction  $\hat{y}_{\sigma(i)}$  for the bipartite matching is:  $\mathcal{L}_{\text{match}}(y_i, \hat{y}_{\sigma(i)}) = -\mathbb{1}_{\{c_i \neq \emptyset\}}\hat{p}_{\sigma(i)}(c_i) + \mathbb{1}_{\{c_i \neq \emptyset\}}\mathcal{L}_{\text{box}}(b_i, \hat{b}_{\sigma(i)})$ , where  $c_i$  is the target class label,  $b_i$  is the target box,  $\hat{b}_{\sigma(i)}$  and  $\hat{p}_{\sigma(i)}(c_i)$  are the predicted box and predicted probability of class  $c_i$ , respectively.

After the bipartite matching, we get the optimal assignment  $\hat{\sigma}$ . We compute the query classification loss  $\mathcal{L}_{\text{cls}}$  and query coordinate regression loss  $\mathcal{L}_{\text{coord}}$  as follows:

$$\mathcal{L}_{\text{cls}} = \sum_{i=1}^N -\log \hat{p}_{\hat{\sigma}(i)}(c_i), \quad \mathcal{L}_{\text{coord}} = \sum_{i=1}^N \mathbb{1}_{\{c_i \neq \emptyset\}} \mathcal{L}_{\text{box}}(b_i, \hat{b}_{\hat{\sigma}(i)}), \quad (1)$$

where  $\mathcal{L}_{\text{box}}$  is the  $\ell_1$  loss for bounding box parameters.

### 3.2 Query-based Prediction

Typical trajectory prediction models can be divided into three components: agent encoder that extracts agent trajectory features, map encoder that extracts map features, and trajectory decoder that outputs predicted trajectories. Different from these models, the query-based detection and tracking module gives tracked agent queries, which is equivalent to the output of the agent encoder. Therefore, the remaining tasks of the query-based prediction module are map encoding and trajectory decoding.

### 3.2.1 Map Encoder

HD semantic maps are crucial for trajectory prediction since they include detailed road information, such as lane types, road boundaries and traffic signs. HD maps are typically represented by vectorized spatial coordinates of map elements and the topological relations between them. To encode this information, we adopt a popular vectorized encoding method VectorNet [38]. Compared with rasterized encoding methods which render maps and agents on an image and extract image features using CNNs, vectorized encoding methods abstract all the map elements and efficiently model their spatial and topological relationships. The map encoder produces a set of map features  $\mathbf{M}$ , which further interacts with agent queries via cross attention:  $\mathbf{Q} = \text{Attention}(\mathbf{Q}, \mathbf{M})$ .

### 3.2.2 Trajectory Decoding

The trajectory decoding takes in the agent queries, and outputs  $K$  possible future trajectories for each agent. ViP3D is compatible with a variety of trajectory decoding methods, such as regression-based methods [39, 40, 41, 31], goal-based methods [25] and heatmap-based methods [26, 27, 42]. We introduce the key ideas of these methods here and leave the details in the Appendix. (1) The regression-based method, namely variety loss, predicts future trajectories based on regression. During inference, this decoder directly outputs a set of predicted trajectories. During training, we first calculate the distance between each predicted trajectory and ground truth trajectory. Then we select a predicted trajectory with the closest distance and only calculate regression loss between it and the ground truth trajectory. (2) The goal-based method first defines sparse goal anchors heuristically, and then classifies these anchors to estimate and select the goals. Finally, a trajectory is completed for each selected goal. (3) The heatmap-based method first generates a heatmap indicating the probability distribution of the goal. Then a greedy algorithm or a neural network is used to select goals from the heatmap. Finally, same as the goal-based method, the trajectories are completed. We use  $\mathcal{L}_{\text{trajectory}}$  to denote the loss of trajectory decoding and leave the detailed definition in the Appendix.

### 3.3 Loss

ViP3D is trained end-to-end with query classification loss and query coordinate regression loss of the query-based detection and tracking module, and trajectory decoding loss of the query-based prediction module:  $\mathcal{L} = \mathcal{L}_{\text{cls}} + \mathcal{L}_{\text{coord}} + \mathcal{L}_{\text{trajectory}}$ .

## 4 Experiments

### 4.1 Experimental Settings

**Dataset.** We train and evaluate ViP3D on the nuScenes dataset, a large-scale driving dataset including the urban scenarios in Boston and Singapore. It contains 1000 scenes, and each scene has a duration of around 20 seconds. The full dataset has more than one million images from 6 cameras and 1.4M bounding boxes for different types of objects. Bounding boxes of objects are annotated at 2Hz over the entire dataset.

**End-to-end Prediction Accuracy.** To evaluate the performance of multi-future trajectory prediction, we adopt the common metrics including minimum average displacement error (minADE), minimum final displacement error (minFDE), and miss rate (MR). However, the inputs of end-to-end prediction are raw videos, so false positive agent detections in end-to-end prediction are not considered in these metrics. Therefore, we propose a more comprehensive evaluation metric for end-to-end visual trajectory prediction, named End-to-end Prediction Accuracy (EPA).

Let us denote predicted and ground truth agents as unordered sets  $\hat{\mathcal{S}}$  and  $\mathcal{S}$ , respectively, where each agent is represented by  $K$  future trajectories of different modalities. First, for each agent type  $c$ , we calculate the prediction precision between  $\hat{\mathcal{S}}_c$  and  $\mathcal{S}_c$ , where the subscript  $c$  indicates the agents of type  $c$ . We define the cost between a predicted agent  $\hat{s}$  and a ground truth agent  $s$  as:

$$C_{\text{EPA}}(s, \hat{s}) = \begin{cases} \|s_0 - \hat{s}_0\|, & \text{if } \|s_0 - \hat{s}_0\| \leq \tau_{\text{EPA}} \\ \infty, & \text{if } \|s_0 - \hat{s}_0\| > \tau_{\text{EPA}} \end{cases}, \quad (2)$$

where  $\hat{s}_0$  and  $s_0$  indicate the coordinates of the ground truth agent and the predicted agent at the current time step, and we set the threshold for successful matching to  $\tau_{\text{EPA}} = 2.0\text{m}$ . We utilize bi-

Table 1: Comparing ViP3D with traditional multi-stage pipeline under regression-based trajectory decoding. Classical metrics include minADE, minFDE and Miss Rate (MR), and End-to-end Prediction Accuracy (EPA) which is the proposed metric for our end-to-end setting. For each agent, 6 future trajectories with a time horizon of 6 seconds are evaluated.

Pipeline	Tracking inputs	Prediction inputs	minADE↓	minFDE↓	MR↓	EPA ↑
Traditional	Agent boxes	Agent trajectories	2.30	3.33	0.282	0.186
PnPNet-vision [4]	Agent queries	Cropped features	2.22	3.17	0.272	0.193
ViP3D (ours)	Agent queries	Agent queries	<b>2.05</b>	<b>2.84</b>	<b>0.246</b>	<b>0.226</b>

partite matching according to  $C_{\text{EPA}}$  to find the correspondence between predicted agents and ground truth agents. Then the number of false-positive predicted agents is  $N_{\text{FP}} = |\hat{\mathcal{S}}| - |\hat{\mathcal{S}}_{\text{match}}|$ , where  $\hat{\mathcal{S}}_{\text{match}} \subset \hat{\mathcal{S}}$  is the set of predicted agents which have been matched with ground truth agents. For each matched agent, we follow the standard prediction metric and calculate minFDE (minimum final displacement error) between its predicted multiple future trajectories and the ground truth trajectory  $\text{minFDE}(\hat{\mathbf{s}}, \mathbf{s}) = \min_{k \in 1 \dots K} \|\hat{\mathbf{s}}_{T_{\text{future}}}^{(k)} - \mathbf{s}_{T_{\text{future}}}\|$ , where  $\hat{\mathbf{s}}^{(k)}$  is the  $k^{\text{th}}$  trajectory of the matched agent  $\hat{\mathbf{s}}$ , and  $T_{\text{future}}$  is the final time step of the future trajectory. Now the set of agents which have matched and hit a ground truth agent is  $\hat{\mathcal{S}}_{\text{match, hit}} = \{\hat{\mathbf{s}} : \hat{\mathbf{s}} \in \hat{\mathcal{S}}_{\text{match}}, \text{minFDE}(\hat{\mathbf{s}}, \mathbf{s}) \leq \tau_{\text{EPA}}\}$ . The EPA between  $\hat{\mathcal{S}}_c$  and  $\mathcal{S}_c$  is defined as:

$$\text{EPA}(\hat{\mathcal{S}}_c, \mathcal{S}_c) = \frac{|\hat{\mathcal{S}}_{\text{match, hit}}| - \alpha N_{\text{FP}}}{N_{\text{GT}}}, \quad (3)$$

where  $N_{\text{GT}}$  is the number of ground truth agents, and we set penalty coefficient  $\alpha = 0.5$  for all experiments. For different scenes, each number in the equation is defined as the sum over all scenes. Finally, the average EPA between  $\hat{\mathcal{S}}$  and  $\mathcal{S}$  is the average of all agent types.

## 4.2 Baseline Settings

**Traditional Perception and Prediction Pipeline.** The traditional pipeline has independently trained tracker and trajectory predictor. In our experiment, this baseline uses the same query-based tracker and query-based prediction module as ViP3D for a fair comparison. Compared with ViP3D, the outputs of the tracker are agent attributes and states instead of agent queries. These agent attributes and states are manually-defined in common tracking tasks, and we use as many attributes as possible. They include historical trajectories, agent types, agent sizes, agent velocities, *etc.*

**PnPNet-vision.** PnPNet [4] only takes LiDAR data as input, and it cannot be directly used for our visual trajectory prediction task. To fairly compare our ViP3D with PnPNet, we implement *PnPNet-vision* by replacing the LiDAR encoder of the original PnPNet with DETR3D, which is the same as ViP3D.

## 4.3 Evaluation and Analysis

### 4.3.1 Main Results

We compare our ViP3D with PnPNet-vision and traditional perception and prediction pipeline on the nuScenes dataset, as shown in Table 1. We can see that ViP3D outperforms these baselines, indicating the effectiveness and superiority of ViP3D. It also demonstrates the benefit of directly learning from visual information with a fully differentiable approach.

### 4.3.2 Ablation Study

**Trajectory Prediction.** To better understand the necessity of visual features and end-to-end training, we compare ViP3D with different baselines. These baselines have the same architecture as ViP3D except for the prediction inputs. We use the default regression-based method for trajectory decoding. Metrics averaged over vehicles and pedestrians are used to compare their performance on visual trajectory prediction task. Results are shown in Table 2. It can be seen that *Agent trajectories + Agent queries* outperforms *Agent trajectories*, demonstrating that the visual features provide



Table 2: Ablation study on the inputs of trajectory prediction. Trajectory decoding is default to regression-based method.

	Prediction inputs		Differentiable	minADE ↓	minFDE ↓	MR ↓	EPA ↑
	Agent trajectories	Agent queries					
	✓	✗	✗	2.30	3.33	0.282	0.186
	✓	✓	✗	2.20	3.19	0.274	0.211
<b>ViP3D</b>	✗	✓	✓	<b>2.05</b>	<b>2.84</b>	<b>0.246</b>	<b>0.226</b>

more fine-grained and detailed information to improve prediction performance. ViP3D surpasses *Agent trajectories* and *Agent trajectories + Agent queries*, demonstrating that end-to-end learning is helpful in avoiding the error accumulation problem in the multi-stage pipeline.

**Trajectory Decoding.** We also compare our ViP3D with traditional perception and prediction pipeline under other trajectory decoding methods, as shown in Table 3. It demonstrates that ViP3D is compatible with a variety of trajectory decoding methods.

Table 3: Comparing trajectory prediction performance on the nuScenes validation set with another two decoding methods: goal-based and heatmap-based. Except for the trajectory decoding methods, other experimental settings are the same as those in the regression-based method shown in Table 1.

Trajectory Decoding	Pipeline	minADE↓	minFDE↓	MR↓	EPA ↑
Goal-based [25]	Traditional	2.50	3.93	0.266	0.195
	ViP3D (ours)	<b>2.20</b>	<b>3.32</b>	<b>0.247</b>	<b>0.213</b>
Heatmap-based [27]	Traditional	2.53	3.81	0.264	0.197
	ViP3D (ours)	<b>2.33</b>	<b>3.42</b>	<b>0.218</b>	<b>0.214</b>

**Tracking.** We also compare the tracking performance between a separately trained tracker and the tracker of our end-to-end trained ViP3D. These trackers have the same architecture, only the training strategies differ. Results in Table 4 show that the our end-to-end trained tracker slightly outperforms the separately trained tracker.

### 4.3.3 Qualitative Results

We provide examples of the predicted results by ViP3D and traditional pipeline in Figure 3. In the upper example, we can see that the left turn signal of the vehicle in the blue box is flashing, indicating that the vehicle is about to turn left. ViP3D can use this visual information to predict the correct trajectory. In contrast, the traditional pipeline can only use historical trajectory information to predict that the vehicle is about to go straight incorrectly. In the lower example, we can see that the pedestrian is facing the coming vehicle, indicating that he has probably noticed the approaching vehicle and will stop and wait for the vehicle to go first. ViP3D makes use of the pedestrian’s body orientation to correctly predict that the pedestrian will stop, while the traditional pipeline incorrectly predicts that pedestrians will cross the road. These two examples show that ViP3D improves trajectory prediction performance due to utilizing visual information.

## 5 Conclusion

We present ViP3D, a fully differentiable and streaming approach to predict future trajectories of agents from multi-view videos. It exploits the rich visual information from the raw sensory input,

Table 4: Ablation study comparing the performance of the tracker in ViP3D and the one trained separately.

Tracker	AMOTA	AMOTP	Recall
Separately-trained	0.216	1.616	0.358
ViP3D	0.217	1.625	0.363

and avoids the error accumulation problem in the traditional pipeline. Moreover, by leveraging 3D agent queries, ViP3D models agent instances explicitly, making the pipeline interpretable and debuggable.



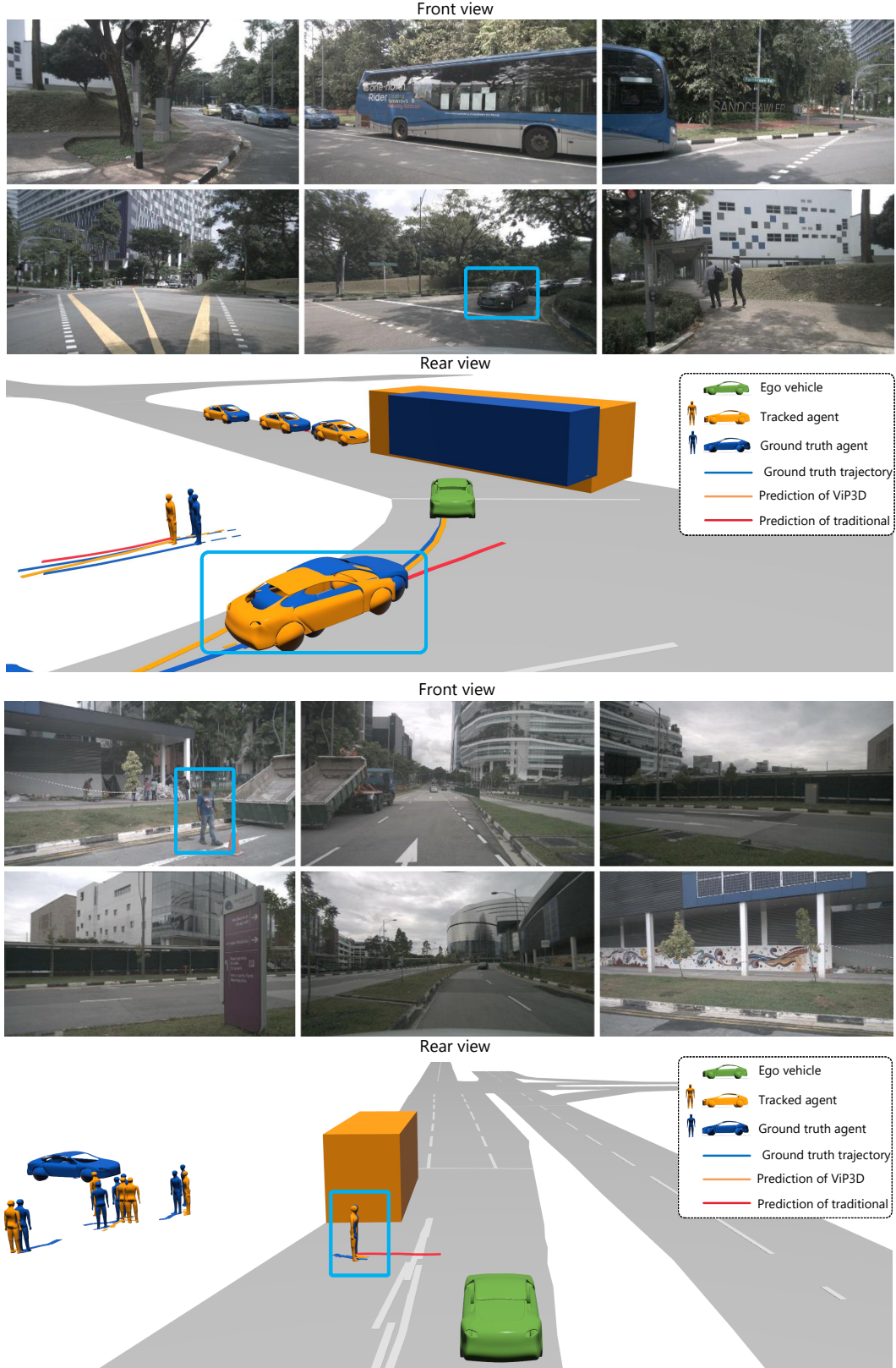


Figure 3: Qualitative results. Input camera images are shown on the top. The green vehicle is the ego agent. The blue and orange agents indicate ground-truth and tracked agents, respectively. The blue, orange and red curves indicate ground-truth trajectories, prediction of ViP3D and prediction of traditional pipeline, respectively. For each agent, only the predicted trajectory with the highest probability is drawn.

## References

- [1] P. Zhang, L. Bai, J. Xue, J. Fang, N. Zheng, and W. Ouyang. Trajectory forecasting from detection with uncertainty-aware motion encoding. *arXiv preprint arXiv:2202.01478*, 2022.
- [2] S. Casas, W. Luo, and R. Urtasun. Intentnet: Learning to predict intention from raw sensor data. In *Conference on Robot Learning*, pages 947–956. PMLR, 2018.
- [3] W. Luo, B. Yang, and R. Urtasun. Fast and furious: Real time end-to-end 3d detection, tracking and motion forecasting with a single convolutional net. In *Proceedings of the IEEE conference on Computer Vision and Pattern Recognition*, pages 3569–3577, 2018.
- [4] M. Liang, B. Yang, W. Zeng, Y. Chen, R. Hu, S. Casas, and R. Urtasun. Pnpnet: End-to-end perception and prediction with tracking in the loop. In *Proceedings of the IEEE/CVF Conference on Computer Vision and Pattern Recognition*, pages 11553–11562, 2020.
- [5] C. R. Qi, H. Su, K. Mo, and L. J. Guibas. PointNet: Deep Learning on Point Sets for 3D Classification and Segmentation. In *CVPR*, pages 652–660, 2017.
- [6] Y. Zhou and O. Tuzel. VoxelNet: End-to-End Learning for Point Cloud Based 3D Object Detection. In *CVPR*, pages 4490–4499, 2018.
- [7] A. H. Lang, S. Vora, H. Caesar, L. Zhou, J. Yang, and O. Beijbom. PointPillars: Fast Encoders for Object Detection from Point Clouds. In *CVPR*, pages 12697–12705, 2019.
- [8] A. Simonelli, S. R. Bulo, L. Porzi, M. López-Antequera, and P. Kotschieder. Disentangling monocular 3d object detection. In *Proceedings of the IEEE/CVF International Conference on Computer Vision*, pages 1991–1999, 2019.
- [9] T. Wang, X. Zhu, J. Pang, and D. Lin. Fcos3d: Fully convolutional one-stage monocular 3d object detection. *arXiv preprint arXiv:2104.10956*, 2021.
- [10] Y. Wang, W.-L. Chao, D. Garg, B. Hariharan, M. Campbell, and K. Q. Weinberger. Pseudo-LiDAR from Visual Depth Estimation: Bridging the Gap in 3D Object Detection for Autonomous Driving. In *CVPR*, pages 8445–8453, 2019.
- [11] Y. Wang, V. C. Guizilini, T. Zhang, Y. Wang, H. Zhao, and J. Solomon. Detr3d: 3d object detection from multi-view images via 3d-to-2d queries. In *5th Annual Conference on Robot Learning*, 2021.
- [12] Z. Li, W. Wang, H. Li, E. Xie, C. Sima, T. Lu, Q. Yu, and J. Dai. Bevformer: Learning bird’s-eye-view representation from multi-camera images via spatiotemporal transformers. *arXiv preprint arXiv:2203.17270*, 2022.
- [13] X. Weng, J. Wang, D. Held, and K. Kitani. 3D Multi-Object Tracking: A Baseline and New Evaluation Metrics. *IROS*, 2020.
- [14] Z. Pang, Z. Li, and N. Wang. Simpletrack: Understanding and rethinking 3d multi-object tracking. *arXiv preprint arXiv:2111.09621*, 2021.
- [15] X. Zhou, V. Koltun, and P. Krähenbühl. Tracking objects as points. In *European Conference on Computer Vision*, pages 474–490. Springer, 2020.
- [16] T. Yin, X. Zhou, and P. Krähenbühl. Center-based 3D Object Detection and Tracking. *arXiv preprint arXiv:2006.11275*, 2020.
- [17] S. Scheidegger, J. Benjaminsson, E. Rosenberg, A. Krishnan, and K. Granström. Mono-camera 3d multi-object tracking using deep learning detections and pmbm filtering. In *2018 IEEE Intelligent Vehicles Symposium (IV)*, pages 433–440. IEEE, 2018.
- [18] M. Chaabane, P. Zhang, J. R. Beveridge, and S. O’Hara. Deft: Detection embeddings for tracking. *arXiv preprint arXiv:2102.02267*, 2021.
- [19] H.-N. Hu, Y.-H. Yang, T. Fischer, T. Darrell, F. Yu, and M. Sun. Monocular quasi-dense 3d object tracking. *arXiv preprint arXiv:2103.07351*, 2021.

- [20] T. Zhang, X. Chen, Y. Wang, Y. Wang, and H. Zhao. Mutr3d: A multi-camera tracking framework via 3d-to-2d queries. In *Proceedings of the IEEE/CVF Conference on Computer Vision and Pattern Recognition*, pages 4537–4546, 2022.
- [21] J. Hong, B. Sapp, and J. Philbin. Rules of the road: Predicting driving behavior with a convolutional model of semantic interactions. In *Proceedings of the IEEE/CVF Conference on Computer Vision and Pattern Recognition*, pages 8454–8462, 2019.
- [22] R. A. Yeh, A. G. Schwing, J. Huang, and K. Murphy. Diverse generation for multi-agent sports games. In *Proceedings of the IEEE/CVF Conference on Computer Vision and Pattern Recognition*, pages 4610–4619, 2019.
- [23] C. Sun, P. Karlsson, J. Wu, J. B. Tenenbaum, and K. Murphy. Stochastic prediction of multi-agent interactions from partial observations. *arXiv preprint arXiv:1902.09641*, 2019.
- [24] Y. C. Tang and R. Salakhutdinov. Multiple futures prediction. *arXiv preprint arXiv:1911.00997*, 2019.
- [25] H. Zhao, J. Gao, T. Lan, C. Sun, B. Sapp, B. Varadarajan, Y. Shen, Y. Shen, Y. Chai, C. Schmid, et al. Tnt: Target-driven trajectory prediction. *arXiv preprint arXiv:2008.08294*, 2020.
- [26] J. Gu, C. Sun, and H. Zhao. Densetnt: End-to-end trajectory prediction from dense goal sets. In *Proceedings of the IEEE/CVF International Conference on Computer Vision*, pages 15303–15312, 2021.
- [27] T. Gilles, S. Sabatini, D. Tsishkou, B. Stanciulescu, and F. Moutarde. Home: Heatmap output for future motion estimation. *arXiv preprint arXiv:2105.10968*, 2021.
- [28] T. Gilles, S. Sabatini, D. Tsishkou, B. Stanciulescu, and F. Moutarde. Thomas: Trajectory heatmap output with learned multi-agent sampling. In *International Conference on Learning Representations*, 2021.
- [29] H. Song, D. Luan, W. Ding, M. Y. Wang, and Q. Chen. Learning to predict vehicle trajectories with model-based planning. *arXiv preprint arXiv:2103.04027*, 2021.
- [30] B. Kim, S. H. Park, S. Lee, E. Khoshimjonov, D. Kum, J. Kim, J. S. Kim, and J. W. Choi. LaPred: Lane-aware prediction of multi-modal future trajectories of dynamic agents. In *Proceedings of the IEEE/CVF Conference on Computer Vision and Pattern Recognition*, pages 14636–14645, 2021.
- [31] M. Liang, B. Yang, R. Hu, Y. Chen, R. Liao, S. Feng, and R. Urtasun. Learning lane graph representations for motion forecasting. In *European Conference on Computer Vision*, pages 541–556. Springer, 2020.
- [32] J. Phillips, J. Martinez, I. A. Barsan, S. Casas, A. Sadat, and R. Urtasun. Deep multi-task learning for joint localization, perception, and prediction. In *Proceedings of the IEEE/CVF Conference on Computer Vision and Pattern Recognition (CVPR)*, pages 4679–4689, June 2021.
- [33] A. Hu, Z. Murez, N. Mohan, S. Dudas, J. Hawke, V. Badrinarayanan, R. Cipolla, and A. Kendall. Fiery: Future instance prediction in bird’s-eye view from surround monocular cameras. In *Proceedings of the IEEE/CVF International Conference on Computer Vision*, pages 15273–15282, 2021.
- [34] F. Zeng, B. Dong, T. Wang, X. Zhang, and Y. Wei. Motr: End-to-end multiple-object tracking with transformer. *arXiv preprint arXiv:2105.03247*, 2021.
- [35] K. He, X. Zhang, S. Ren, and J. Sun. Deep Residual Learning for Image Recognition. In *CVPR*, pages 770–778, 2016.
- [36] T.-Y. Lin, P. Dollár, R. Girshick, K. He, B. Hariharan, and S. Belongie. Feature Pyramid Networks for Object Detection. In *CVPR*, pages 2117–2125, 2017.
- [37] N. Carion, F. Massa, G. Synnaeve, N. Usunier, A. Kirillov, and S. Zagoruyko. End-to-end object detection with transformers. In *ECCV*, 2020.

- [38] J. Gao, C. Sun, H. Zhao, Y. Shen, D. Anguelov, C. Li, and C. Schmid. Vectornet: Encoding hd maps and agent dynamics from vectorized representation. In *Proceedings of the IEEE/CVF Conference on Computer Vision and Pattern Recognition*, pages 11525–11533, 2020.
- [39] A. Gupta, J. Johnson, L. Fei-Fei, S. Savarese, and A. Alahi. Social gan: Socially acceptable trajectories with generative adversarial networks. In *Proceedings of the IEEE Conference on Computer Vision and Pattern Recognition*, pages 2255–2264, 2018.
- [40] H. Cui, V. Radosavljevic, F.-C. Chou, T.-H. Lin, T. Nguyen, T.-K. Huang, J. Schneider, and N. Djuric. Multimodal trajectory predictions for autonomous driving using deep convolutional networks. In *2019 International Conference on Robotics and Automation (ICRA)*, pages 2090–2096. IEEE, 2019.
- [41] C. Rupprecht, I. Laina, R. DiPietro, M. Baust, F. Tombari, N. Navab, and G. D. Hager. Learning in an uncertain world: Representing ambiguity through multiple hypotheses. In *Proceedings of the IEEE international conference on computer vision*, pages 3591–3600, 2017.
- [42] T. Gilles, S. Sabatini, D. Tsishkou, B. Stanciulescu, and F. Moutarde. Gohome: Graph-oriented heatmap output for future motion estimation. *arXiv preprint arXiv:2109.01827*, 2021.
- [43] M.-F. Chang, J. Lambert, P. Sangkloy, J. Singh, S. Bak, A. Hartnett, D. Wang, P. Carr, S. Lucey, D. Ramanan, et al. Argoverse: 3d tracking and forecasting with rich maps. In *Proceedings of the IEEE/CVF Conference on Computer Vision and Pattern Recognition*, pages 8748–8757, 2019.

## A Implementation Details

**Query-based Detection and Tracking.** The query-based detection and tracking module takes ResNet50 [35] as the image backbone and DETR3D [11] as the detection head. The detection head consists of 6 layers, and each layer contains a feature refinement layer and a multi-head attention layer with layer normalization. The hidden size for the detection head is set to 256. Finally, one branch predicts center coordinates and size of agents, and the other branch predicts agent type.

**Trajectory Predictor.** Popular trajectory prediction benchmarks, such as Argoverse Motion Prediction Benchmark [43], require the prediction of one target agent in each scene. A commonly used trick is to normalize the map and the agent trajectories by taking the last position of the target agent as the origin and its direction as  $y$ -axis. This normalization makes prediction models focus on future modality prediction instead of coordinate transformation, thereby improving the prediction performance but limited to predicting one agent at a time. In our visual trajectory prediction task, we simultaneously predict all agents in each scene for a fast inference speed. Although we cannot normalize the maps and the surrounding agents for each target agent, we can predict the offsets between the future trajectories and the current position of the target agent.

**Training and Inference Details.** In our experiments, all models are trained on the nuScenes training set with a batch size of 8 for 24 epochs. The Adam optimizer is adopted to train the whole pipeline. The learning rate has an initial value of  $2e^{-4}$  and decays to 10% at the 20th and the 23rd epochs. The hidden size of the query-based detection and tracking module is set to 256, and that of the trajectory predictor is set to 128. We evaluate all models on the nuScenes validation set. All models are tested online by feeding raw data of each time step to the model in chronological order. The metric computing is performed at every step except for steps that do not have enough future frames. Unlike popular trajectory prediction benchmarks requiring the prediction of selected agents, we simultaneously predict all agents at each step.

## B Trajectory Decoding

ViP3D can leverage a variety of trajectory decoding methods, such as regression-based methods [39, 40, 41, 31], goal-based methods [25] and heatmap-based methods [26, 27, 42]. We conduct experiments on these three trajectory decoding methods. In this section, we introduce the implementation details of these methods.

**Regression-based.** The regression-based trajectory decoder is a 2-layer MLP that takes the agent queries as input and directly outputs multiple future trajectories. During inference, the regression-based trajectory decoder directly outputs a set of predicted trajectories. During training, we first calculate the distance between each predicted trajectory  $\hat{s}$  and ground truth trajectory  $s$ :  $d(s, \hat{s}) = \sum_{t=1}^{T_{\text{future}}} \|s_t - \hat{s}_t\|$ , where  $\|\cdot\|$  is the  $\ell_2$  distance between two points. Then, we select the predicted trajectory with the closest distance:  $\hat{k} = \operatorname{argmin}_{k \in 1 \dots K} d(s, s^{(k)})$ , where  $s^{(k)}$  is the  $k^{\text{th}}$  predicted trajectory. Finally, we calculate regression loss between the closest predicted trajectory  $s^{(\hat{k})}$  and the ground truth trajectory  $s$  as

$$\mathcal{L}_{\text{trajectory}} = \sum_{t=1}^{T_{\text{future}}} \mathcal{L}_{\text{reg}}(s_t, s_t^{(\hat{k})}), \quad (4)$$

where  $\mathcal{L}_{\text{reg}}$  is the smooth  $\ell_1$  loss between two points.

**Goal-based.** The goal-based trajectory decoder consists of a goal encoder, a probability decoder, an offset decoder, and a trajectory completion module. These modules are implemented using MLP. For each agent, we first randomly generate a set of candidate goals. The goal encoder is used to obtain the features of candidate goals by taking their coordinates as input. After that, a concatenation of the agent query and the features of goal coordinates is fed into the probability decoder and offset decoder. The probability decoder and the offset decoder output predicted goal probabilities and goal offsets, respectively. Let  $\mathcal{L}_{\text{cls}}$  be the binary cross-entropy loss for the probability decoder,

and let  $\mathcal{L}_{\text{reg}}$  be the smooth  $\ell_1$  loss for the offset decoder. To obtain  $K$  trajectories, Non-maximum supervision (NMS) is employed to select  $K$  goals (after adding the goal offsets), and the trajectory completion module takes the  $K$  selected goals and outputs  $K$  trajectories. Let  $\mathcal{L}_{\text{completion}}$  be the smooth  $\ell_1$  loss for the trajectory completion module. Then the overall loss is

$$\mathcal{L}_{\text{trajectory}} = \mathcal{L}_{\text{cls}} + \mathcal{L}_{\text{reg}} + \mathcal{L}_{\text{completion}}. \quad (5)$$

**Heatmap-based.** The heatmap-based trajectory decoder only consists of a goal encoder, a probability decoder, and a trajectory completion module. These modules are implemented using MLP. For each agent, to obtain a heatmap indicating the probability distribution of the final positions of the trajectories, we first densely sample goals with a sampling density of 1m. The goal encoder is used to obtain the features of the goals by taking their coordinates as input. After that, a concatenation of the agent query and the features of goal coordinates is fed into the probability decoder. The probability decoder outputs predicted goal probabilities, and we obtain the heatmap. Let  $\mathcal{L}_{\text{cls}}$  be the binary cross-entropy loss for the probability decoder. To obtain  $K$  trajectories, we also use NMS to select  $K$  goals for simplification, instead of using greedy algorithms as in origin heatmap-based methods [27]. The trajectory completion module takes the  $K$  selected goals and outputs  $K$  trajectories. Let  $\mathcal{L}_{\text{completion}}$  be the smooth  $\ell_1$  loss for the trajectory completion module. Then the overall loss is

$$\mathcal{L}_{\text{trajectory}} = \mathcal{L}_{\text{cls}} + \mathcal{L}_{\text{completion}}. \quad (6)$$